ACOUSTICAL EFFECTS OF SURFACE ROUGHNESS

Keith Attenborough Department of Engineering, University of Hull, HU6 7RX, UK
Patrice Boulanger Department of Engineering, University of Hull, HU6 7RX, UK
Qin Qin Department of Engineering, University of Hull, HU6 7RX, UK

1 INTRODUCTION

Surface roughness with scales much smaller than the incident wavelengths influences reflection from the ground in a manner similar to finite impedance. The influence of small-scale roughness on acoustically hard surfaces is to make them acoustically-soft[1]. The effect of small-scale roughness on porous surfaces is mainly to reduce the real part of the impedance[2,3]. One theoretical approach is to consider plane wave reflection and scattering from a surface containing geometrical roughness elements or 'bosses' on a plane surface. Previous papers[1,2] have introduced heuristic boss models as the basis for predicting the effective impedance of rough surfaces. This paper revisits the analytical boss models due to Twersky[4,5] for the acoustical properties of rough-hard and rough-porous surfaces and extends them heuristically. Predictions of the previous and extended models are compared with short-range data obtained in the laboratory and outdoors. Predicted effective impedance spectra are compared with those deduced from EA measurements over unploughed and ploughed sandy soil, rough gravel surfaces and 2-D periodically- rough sand surfaces.

2 'BOSS' MODELS

Several theories have been developed to describe the relative effective impedance ($Z = 1/\beta$) of rough surfaces when the roughness scale is small compared to the incident acoustic wavelengths. The boss theories due to Biot and Tolstoy model rough surfaces of finite impedance but does not account for non-specular scattering and leads to relatively poor agreement with measurements[3]. On the other hand, Twersky[4] has developed a theory that incorporates non-specular scattering. When used to model 2-D periodic and randomly-spaced acoustically-hard roughness, the theory gives reasonable agreement with measured ground effect[1]. This model has been extended heuristically to predict roughness effects on finite impedance materials and gives good agreement with ground effect measured over rough sand surfaces and outdoor ground[2]. The real part of the effective impedance predicted by Twersky's theory for hard rough surfaces does not predict the low frequency limit that is expected from physical considerations i.e. infinite Re(Z). A more general version[5] of Twersky's theory allows for acoustically-soft scatterers in an otherwise acoustically-hard plane. It introduces a term proportional to wave-number k in the Re(β) expansion. The roughness material is modelled as rigid-porous through the introduction of complex compressibility and mass density (ratio) expressions for fluid in the pores[6]. Since the original version of this theory does not agree well with measured data obtained from rough porous surfaces at low frequencies, a heuristic extension of this model is introduced here and compared to the heuristic Biot/Tolstoy/Twersky developed elsewhere[2].

Twersky has presented general expressions[5] for the real and imaginary parts of the effective admittance for 2D or 3D randomly-spaced roughness on a plane. This formulation includes absorption of acoustic energy on reflection and scattering of incident waves by roughness elements of various shapes. The main aspects of Twersky's work are summarized below using notation consistent with other published work about effects of acoustically-hard roughness[1].

The direction cosines of the incident wave vector $\boldsymbol{k}$, are represented by γ_i. Note that when the index i used in this work runs from 1 to 3 and refers to the axes z,x,y. If φ is the azimuthal angle and α is the angle between $\boldsymbol{k}$ and the vertical axis z then $\gamma_1 = \cos(\alpha)$, $\gamma_2 = \sin(\alpha)\cos(\varphi)$, $\gamma_3 = \sin(\alpha)\sin(\varphi)$. The roughness properties are specified by relative compressibility κ and (normalised) inverse mass density B_i. In general these are complex.

Twersky introduces

$$C = \kappa - 1 \tag{1}$$

and

$$B'_i = -(B_i - 1)/(1 + (B_i - 1)Q_i), \tag{2}$$

so that real and imaginary parts of B'_i and C are given by

$$B'_i = B'_{i(1)} - iB'_{i(2)} \tag{3}$$

and

$$C = C_{(1)} + iC_{(2)} \tag{4}$$

The real components $C_{(2)}$ and $B'_{i(2)}$ are positive and small compared to $C_{(1)}$ and $B'_{i(1)}$. $Q_i = q_i + \varepsilon_i$ is the depolarization factor expressed in terms of the shape integral q_i and the depolarization due to randomness ε_i. The shape factor can be expressed in terms of the principal diameters of the roughness elements and ε_i depends on integral equations involving the packing factor of the random roughness distribution. The density of roughness elements is denoted by n, the wave number magnitude is k and the roughness cross section area is U. The imaginary part of the surface admittance β is given by:

$$\mathrm{Im}(\beta_{\pm}) = -\frac{nU}{2} k\Phi^{\pm}_1 \tag{5}$$

$$\Phi^{+}_1 = C_{(1)} + B'_{2(1)}\gamma_2^2 - B'_{3(1)}\gamma_3^2 \tag{6}$$

and

$$\Phi^{-}_1 = -B'_{1(1)}\gamma_1^2 \tag{7}$$

The +/- subscripts indicate hard or pressure release surfaces respectively. The real part of the admittance based on Twersky's relations (6.95) involves absorption and scattering terms given by:

$$\mathrm{Re}(\beta_{\pm}) = -\frac{nU}{2} k\Phi^{\pm}_a - \frac{nW_s U^2}{8}(k^3, \frac{k^4}{\pi})\Phi^{\pm}_S \tag{8}$$

$$\Phi^{+}_a = C_{(2)} + B'_{2(2)}\gamma_2^2 + B'_{3(2)}\gamma_3^2 \tag{9}$$

$$\Phi^{-}_a = B'_{1(2)}\gamma_1^2 \tag{10}$$

$$\Phi^{+}_s = C_{(1)}{}^2 + \frac{B'^2_{2(1)}\gamma_2^2}{m} + \frac{B'^2_{3(1)}\gamma_3^2}{m} \tag{11}$$

$$\Phi^{-}_s = \frac{B'^2_{1(1)}\gamma_1^2}{m} \tag{12}$$

the values (k^3 , $m = 2$) and (k^4 , $m = 3$) are used for 2D and 3D roughness respectively. The packing factor, W_s, can be expressed in terms of integrals of the Zernicke-Prins pair functions. Approximations can be obtained in terms of the packing density W of the corresponding distribution of scatterers. Expressions are given below for 2D semi-cylindrical and 3D hemi-spherical roughness. In general, a dyadic parameter $\boldsymbol{B}$ for inverse mass density is used, and incorporates the shape integrals q_i in a dyadic $\mathbf{q}$ but it is assumed here that the principal axes of all dyadics are aligned with the Cartesian axes and B_i are used instead. Since interest here is in rigid porous roughness rather than pressure release surfaces, expressions previously presented with the superscript + are used exclusively.

Consider 2-D circular semi-cylindrical roughness with axes parallel to y. The azimuthal angle φ is zero and the plane-wave incidence angle α is measured from the vertical axis z. Consequently, the direction cosines are expressed by $\gamma_1 = \cos\alpha$ and $\gamma_2 = \sin\alpha$. The third direction cosine is $\gamma_3 = 0$ therefore, the factors depending on the index i = 3 are irrelevant in 2D. For cylindrical roughness, the packing factor is $W_s = (1-W)^2$ where the packing density $W = nb^* = \frac{b^*}{b}$ and b is the average roughness separation distance. b^* is the radius of the exclusion region around a scatterer which i.e. the minimum distance between two scatterer centres in 2D. Twersky has expressed the depolarization factors $Q_i = q_i + \varepsilon_i$ in two dimensions in terms of the shape integrals for circular cylinders $q_1 = q_2 = 1/2$, $q_3 = 0$ and the randomness depolarization $\varepsilon_1 = -\varepsilon_2 = U I_2/2\pi b^{*2}$ for cylindrical

dipoles. If the radius of the circular semi-cylindrical roughness is *a* and *n* is the number of semi-cylinders per unit length (= 1/*b*), the raised cross sectional area per unit length $V = n\pi a^2 / 2 =$ *nU*/2. Hence the depolarization factor for circular semi-cylinders becomes $Q_i = \frac{1}{2} - \frac{I_2 V}{2\pi b_*^{\,2}}$. The expression for I_2 is

$$I_2 \cong 2W\left(1 + 0.307W + 0.137W^2\right) \qquad \text{for } W < 0.8,$$

$$I_2 \cong \frac{\pi^2}{3}\left[1 - \frac{2(1-W)}{W}\right] + 6\frac{(1-W)^2}{W^2}\left[\frac{\pi^2}{6} + 1.202\right] \qquad \text{for } W \geq 0.8$$

$$I \cong \frac{(\pi a)^2}{3b^2} \qquad \text{for } W = 1 \text{ (periodic),}$$

The effective admittance β (relative to air) of a rough surface containing randomly spaced 2D porous circular semi-cylinders is deduced from relations (5) and (8) as

$$\beta_{2D} = \eta_{2D} - i\xi_{2D}. \tag{11}$$

where

$$\xi_{2D} = kV\left\{C_1 - \mathrm{Re}\left[\frac{B-1}{1+(B-1)Q_i}\right]\sin^2\alpha\right\} \tag{12}$$

and

$$\eta_{2D} = kV\left\{C_2 - \mathrm{Im}\left[\frac{B-1}{1+(B-1)Q_i}\right]\sin^2\alpha\right\} + k^3(1-W)^2\frac{V^2}{2n}\left\{C_1^2 + \frac{1}{2}\mathrm{Re}\left[\frac{B-1}{1+(B-1)Q_i}\right]^2\sin^2\alpha\right\} \tag{13}$$

It is straightforward to recover the effective impedance obtained for rigid roughness. Indeed, if the inverse mass density ratio $B \to 0$ and the roughness material is incompressible, then $\kappa_r << \kappa_a$ implying $C_{(1)} = -1$ and $C_{(2)}=0$. Assuming air-filled bosses i.e. no roughness, the parameters $C_1 = \mathrm{Re}(\kappa_r/\kappa_a - 1)$ and $C_2 = \mathrm{Im}(\kappa_r/\kappa_a)$ tend to zero when the roughness compressibility becomes close to air. The relative inverse mass density *B* becomes 1, and the effective admittance due to the roughness is zero as is expected for a smooth hard surface. Note also that this result corroborates the fact that Twersky's theory models porous roughness imbedded in a flat hard surface.

Similar effective admittance relations can be obtained for semi-elliptical scatterers. Given semi-elliptical cylinders with semi-axis a_1 and a_2, the depolarization factors become $Q_1 = \frac{a_2}{a_1 + a_2} - \frac{I_2 V}{2\pi b_*^{\,2}}$ and $Q_2 = \frac{a_1}{a_1 + a_2} + \frac{I_2 V}{2\pi b_*^{\,2}}$. Only Q_2 is of interest for non-pressure release rough surfaces and the roughness cross section per unit length becomes $V = n\frac{\pi a_h\, a_w}{2}$. These expressions for V and Q_2 are the only modifications to the effective admittance expressions for circular cylinders.

For 3-D hemispherical roughness with vertical axis z, the direction cosines are expressed by $\gamma_1 = \cos(\alpha)$, $\gamma_2 = \sin(\alpha)\cos(\varphi)$ and $\gamma_3 = \sin(\alpha)\sin(\varphi)$ and the packing factor is $W_s = (1-W)^3/(1+W)$. The depolarization factors $Q_i = q_i + \varepsilon_i$ in three dimensions are expressed in terms of the shape integrals for hemi-spheres $q_1 = q_2 = q_3 = 1/3$ and the randomness depolarization $\varepsilon_3 = \varepsilon_2 = -UI_2/8\pi b^3$, assuming that the radius of the exclusion region around a scatterer is isotropic $b^*_3 = b^*_2 = b^*$. Note that only the indices i = 2,3 are of interest for non-pressure release rough surfaces. If the hemi-spherical roughness has radius *a* and density *n* hemi-spheres per unit area, then the raised cross sectional area per unit length $V = 2n\pi a^3/3 = nU/2$. Summing both expressions, the depolarization factor

becomes $Q_i = \frac{1}{3} - \frac{I_2 V}{8\pi b_*^3}$. The expression for the integral I_2 based on 2-D packing of impenetrable circular disks is approximated by the virial expansion I_2 = 8*W*(1.+0.4157*W*) for 0<W<0.84. The upper bound W is the experimental value for the densest random packing of identical circular disks. Note that the packing density can never reach the value W = 1 as for 2-D roughness distributions. The effective admittance $\beta_{3D} = \eta_{3D} - i\xi_{3D}$ relative to air of a rough surface containing randomly spaced 3D porous hemispheres imbedded in a smooth hard surface is

$$\xi_{3D} = kV\left\{C_1 - \mathrm{Re}\left[\frac{B-1}{1+(B-1)Q_i}\right]\sin^2\alpha\right\} \quad (14)$$

and

$$\eta_{3D} = kV\left\{C_2 - \mathrm{Im}\left[\frac{B-1}{1+(B-1)Q_i}\right]\sin^2\alpha\right\} + k^4\frac{(1-W)^3}{1+W}\frac{V^2}{2\pi n}\left\{C_1^2 + \frac{1}{3}\mathrm{Re}^2\left[\frac{B-1}{1+(B-1)Q_i}\right]\sin^2\alpha\right\} \quad (15)$$

Note that Twersky's theory is based on the approximations ka<<1 and kb<<1.

A heuristic combination of boss theories has been derived and tested with measured data over sand, grassland and sub-soiled ground[2]. It is based on the Biot/Tolstoy's theory for specular scattering extended to include a real part of admittance ($\eta_{2D\ TwerHard}$) fromTwersky's theory for 2-D hard surfaces. It may be expressed as

$$\beta_{Heur\ Biot} = \eta_{2D\ TwerHard} - ikV[\,\delta \sin^2\alpha - 1 + \Omega\gamma\,] + \beta_{smooth}. \quad (16)$$

δ is the dipole coupling term $\delta = \frac{2}{1+I}$ with $I = \frac{a^2}{b^{*2}} I_2$ for semi-circular cylindrical roughness.

This expression includes the admittance β_{smooth} of a smooth porous surface. This is crucial in obtaining agreement with measured data at low frequency. The term $\eta_{2D\text{-}TwerHard}$ in (16) may be improved by using a more sophisticated expression. This new heuristic model is based on the assumption that the admittance of porous roughness imbedded in a smooth porous ground is equivalent to summing the admittance of a smooth porous surface and that of porous roughness imbedded in a smooth hard surface. With this hypothesis, the admittance is defined as

$$\beta_{2D,3D} + \beta_{smooth} \quad (17)$$

using either (12,13) or (14,15) together with a smooth porous surface model. Note that even if the admittance of the smooth porous surface does not depend on angle, i.e. if the smooth surface is locally-reacting, the effective admittance of the porous rough surface is dependent on angle.

3 COMPARISONS WITH DATA

Effective impedance spectra have been derived from short-range measurements of complex excess attenuation (EA) from a point source[7]. Such spectra are obtained by numerical solution of the complex admittance equation derived from the classical expression for a point source over an impedance boundary. Data have been obtained outdoors over sandy soil (unploughed and ploughed) and gravel pits have obtained as part of a trial, funded in part by the US Army Corps of Engineers BT-25 program, at a US Army Fort Drum establishment in Northern New York State. The site was an area of approximately 500m×500m of sandy soil covered with vegetation. The gravel was in pits approximately 3.6m×3.6m. Measurements of complex EA were made using a source consisting of mid-range Hi-Fi driver in a cylindrical cabinet and MLSSA (Half Blackman Harris window) for signal acquisition and analysis. Figure 1 shows example data (continuous lines) obtained over (unploughed) vegetation covered sandy soil with source and receiver height at 0.54m and horizontal separation 2m, together with predictions (broken and dotted lines). The formulae for the impedance models are summarized in Table 1 and the parameters used for the fits are shown in Tables 2 and 3. Figure 2 shows the example data and predictions after ploughing (across furrows); source and receiver height at 0.54m, range 3m.

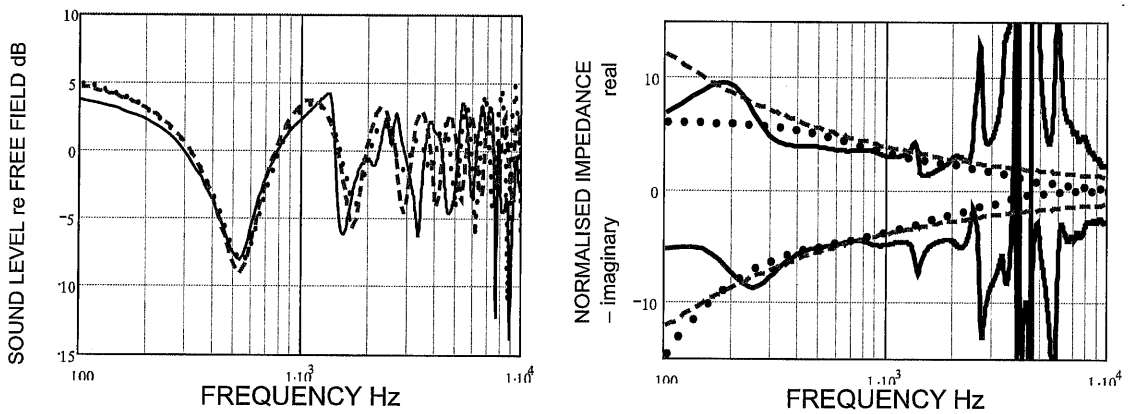

Figure 1 (a) Measured and predicted excess attenuation spectra over vegetation covered sandy soil (b) directly deduced and predicted impedance spectra. See Tables 1 and 2 for models and parameter values.

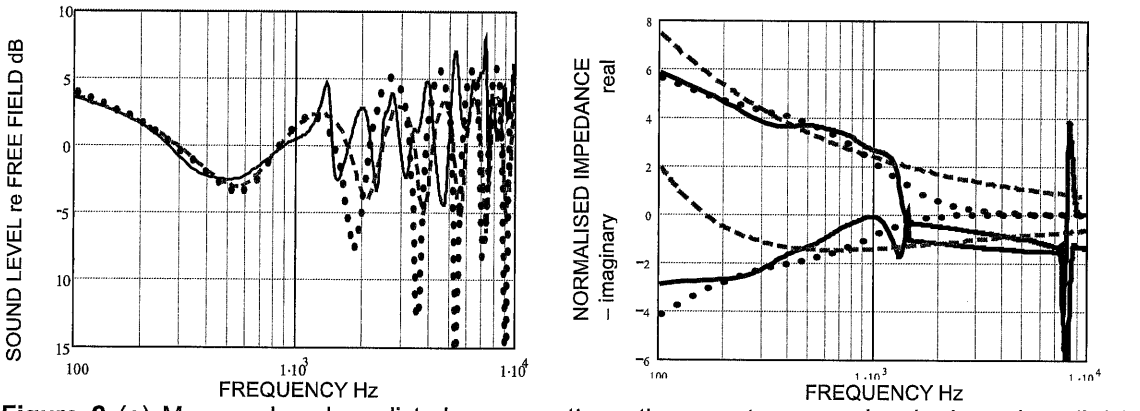

Figure 2 (a) Measured and predicted excess attenuation spectra over ploughed sandy soil (b) directly deduced and predicted impedance spectra. See Tables 1 and 2 for models and parameter values.

Table 1 Formulae for Impedance Models

Model	Parameters	Formulae
2-parameter (variable porosity)	Effective flow resistivity, R_e; porosity change rate, α_e	$Z = \frac{1+i}{\sqrt{\pi\gamma\rho_f}}\sqrt{\frac{R_e}{f}} + \frac{ic_0\alpha_e}{8\pi f}$
Tortuous identical triangular pores with rough surface	Flow resistivity, R_s; Porosity, Ω; Tortuosity, T; layer thickness, roughness height and spacing (see ref. 2)	$\rho(\omega) = \rho_0/H(\lambda)$, $\lambda^2 = \frac{5T\omega\rho_0}{3\Omega R_s}$ $C(\omega) = (\gamma P_0)^{-1}[\gamma - (\gamma-1)H(\lambda\sqrt{(N_{PR})})]$ $H(\lambda) = 1 - 3\coth(\lambda\sqrt{-i})/(\lambda\sqrt{-i}) + 3i/\lambda^2$ $k = \omega[T\rho(\lambda)C(\lambda)]^{0.5}$ $Z_c = (\rho_f c_f)^{-1}[(T/\Omega^2)\rho(\lambda)/C(\lambda)]^{0.5}$
Hard-backed layer	layer thickness, d	$Z(d) = Z_c\coth(-ikd)$

Table 2 Summary of best-fit parameters using the two-parameter impedance model.

Ground	Effective flow resistivity, kPasm^{-2}	porosity change rate, m^{-1}
Unploughed ground	80	0
Ploughed ground (across furrows)	30	–100
Pit 1 (layered gravel)	20	–250
Pit 2 (8 mm gravel)	25	–200

Table 3 Summary of best-fit parameters using equation (16)

3.1 Location	Flow resistivity kPasm^{-2}	Layer depth m	Roughness Height m	Roughness spacing m
Unploughed ground	150	0.05	0.015	0.05
Ploughed ground (across furrows)	20	∞	0.04	0.1
Pit 1 (layered gravel)	0.5	4.5	0.01	0.05
Pit 2 (8 mm gravel)	0.85	1.5	0.005	0.02

In all cases porosity has been assumed to be 0.4 and tortuosity = 1/porosity.

Figures 3 and 4 show results obtained over 'smoothed' gravel surfaces (source and receiver heights 0.56m, range 2m for Pit 1; source and receiver heights at 0.18m, range 2m for Pit 2). Pit 1 consisted of three layers of gravel; the upper layer consisted of 2.5cm stones. Pit 2 consisted of 1.5m depth of 8mm stones.

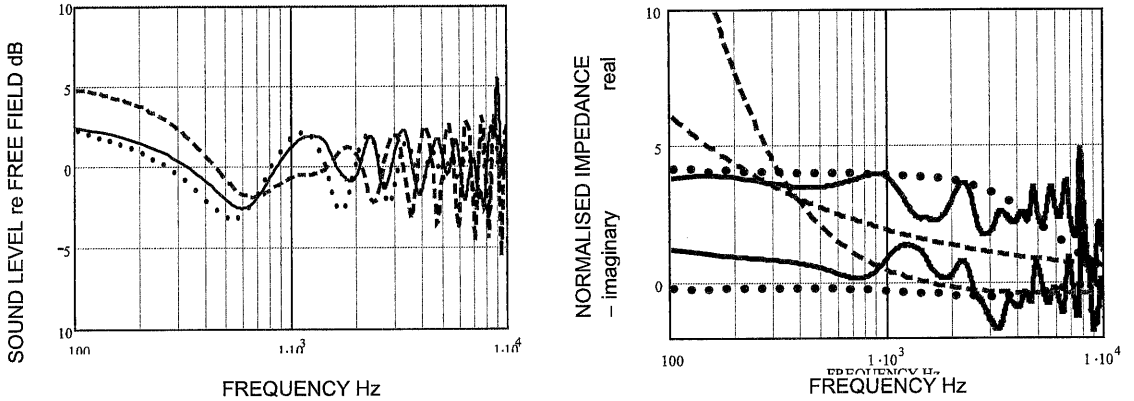

Figure 3 (a) Measured and predicted excess attenuation spectra over a surface composed of large (2.5cm) gravel (b) directly deduced and predicted impedance spectra. See Tables 1 and 2

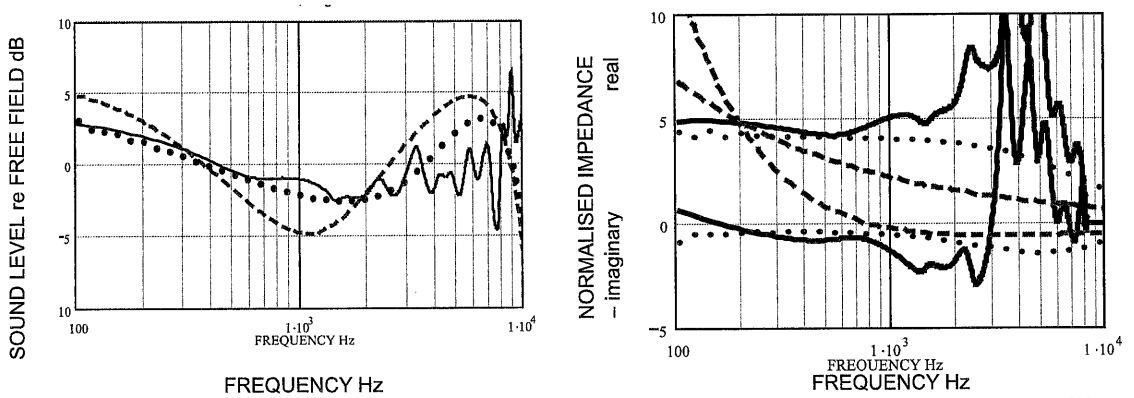

Figure 4 (a) Measured and predicted excess attenuation spectra over a surface composed of 8mm gravel (b) directly deduced and predicted impedance spectra. See Tables 1 and 2 for models and parameter values.

The measured flow resistivity of the 8mm gravel is 850 Pasm^{-2}. Clearly the heuristic boss model (equation (16) gives superior agreement with data, especially for effective impedance spectra deduced above soil after ploughing and the gravel surfaces.

Figure 5 shows impedance spectra (dots) deduced from laboratory measurements, using a point source of broad-band sound, of complex excess attenuation spectra over smooth and rough sand surfaces. The two spectra in each plot correspond to different source and receiver heights (0.2m and 0.1m) at 1m separation. The impedance spectra deduced from measurements over the roughened sand show a significant reduction in the real part and a smaller reduction in the

imaginary part. The sand was wetted before roughening with a shaper. The smooth surface predictions (broken and continuous lines) have been obtained using a slit-pore model[6] with flow resistivity 600 kPasm^{-2}, porosity 0.4 and tortuosity=1/porosity.

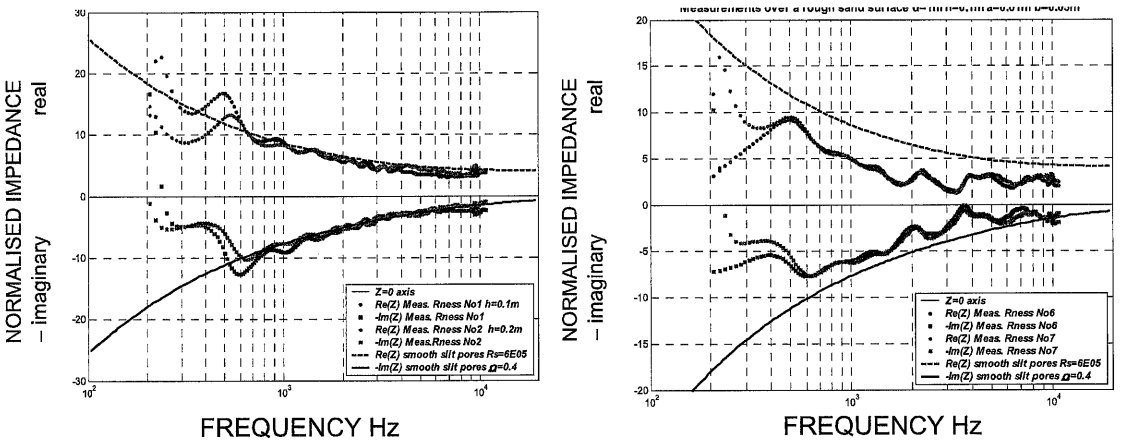

Figure 5 Measured and predicted impedance spectra (a) over a smooth sand surface (b) measured over a sand surface with 'semi-cylindrical' roughness and predicted for the smooth surface.

The nominal roughness characteristic was semi-cylindrical (a=0.01m) and periodic (b=0.005m). Figure 6 shows the impedance spectra deduced from the rough surface data compared with predictions using equations (12, 13) and (16). Figure 7 shows equivalent results using equation (17)

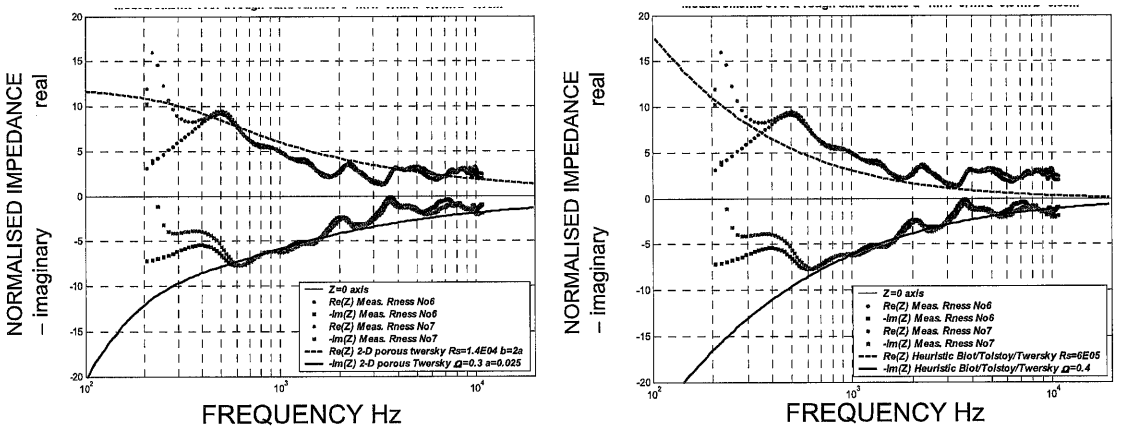

Figure 6 Measured and predicted impedance spectra obtained over a rough sand surface with 'semi-cylindrical' roughness and predictions (a) from equations (12,13) with best-fit parameters and (b) from (16) using nominal parameters.

Using the nominal roughness parameters in equations (12) and (13) does not give good predictions of the measurements. This may be expected since the smooth portions of the sand surface are modelled as hard. A good visual fit is obtained in Figure 6(a) by increasing the semi-cylinder radius to a=0.025m, decreasing flow resistivity to 1.4E04 Pa.s.m^{-2} and decreasing the porosity to Ω=0.3. Use of equation (17) with the nominal sand and roughness parameters gives better agreement (Figure 7(a)) but poorer than obtained with equation (16) (Figure 6(b)). However, the roughness shapes used in the measurements necessarily involved some irregularities due to the difficulty in shaping semi-cylindrical sand roughness. If the roughness is assumed to be semi-elliptical with semi-height a_1=0.006m and semi-width a_2=0.009m then equation (17) gives a good fit to the impedance spectra deduced from measurements.

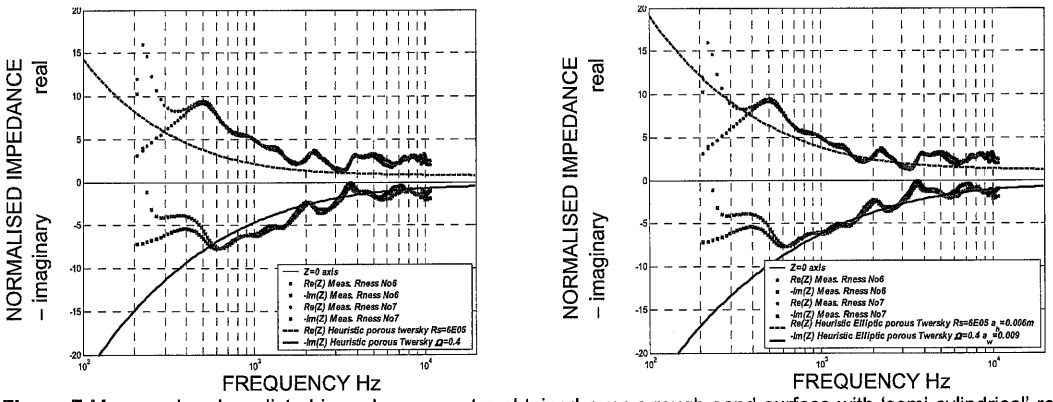

Figure 7 Measured and predicted impedance spectra obtained over a rough sand surface with 'semi-cylindrical' roughness and predictions (a) from equations (17) with circular semi-cylinders and (b) from (17) with elliptic semi-cylinders.

Finally Figure 8 shows impedance spectra for 'soft' hemispheres on 'hard' glass.

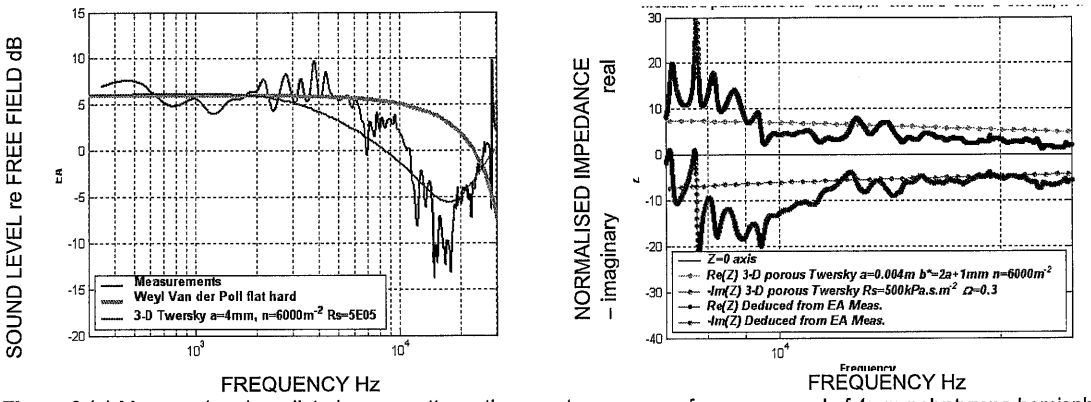

Figure 8 (a) Measured and predicted excess attenuation spectra over a surface composed of 4mm polystyrene hemispheres at a density of 5000 m^2 on a glass plate (b) directly deduced and predicted impedance spectra (equations (14,15)).

4 CONCLUSIONS

Surface roughness at scales rather smaller than the incident wavelengths has an important effect on the apparent impedance of outdoor surfaces. Analytical 'boss' models that include the influence of non-specular scattering may be used to predict the effects. Impedance spectra obtained from short-range measurements of complex excess attenuation are fitted better if roughness is taken into account. A heuristic extension of a model due to Twersky has been found to enable good agreement with impedance spectra obtained from laboratory measurements over rough surfaces.

5 REFERENCES

1. **P. Boulanger, K. Attenborough, S. Taherzadeh, T. Waters-Fuller, and Li K. M., "Ground Effect Over Hard Rough Surfaces". J. Acoust. Soc. Am. 104, 1474-1482 (1998).**
2. **K. Attenborough and T. Waters-Fuller, "Effective impedance of rough porous ground surfaces", J. Acoust. Soc. Am., 108(3) 949-956 (2000)**
3. **K. Attenborough and S. Taherzadeh, "Propagation from a point source over a rough finite impedance boundary", J. Acoust. Soc. Am., 98(3) 1717-22 (1995)**
4. **R. J. Lucas and V. Twersky, "Coherent response to a point source irradiating a rough plane" J. Acoust. Soc. Am. 76, 1847-1863 (1984).**
5. **V. Twersky. "Reflection and scattering of sound by correlated rough surfaces", J. Acoust. Soc. Am. 73, 85-94 (1983).**
6. **K Attenborough, "Models for the acoustical properties of air-saturated granular media" *Acta Acustica* 1 pp 213-226 (1993)**
7. **S. Taherzadeh, and K. Attenborough, "Deduction of ground impedance from measurements of excess attenuation spectra". J. Acoust. Soc. Am. 105, 2039-2042 (1999)**